NeuroImage 265 (2023) 119784

Contents lists available at ScienceDirect

NeuroImage

journal homepage: www.elsevier.com/locate/neuroimage

Cot-side imaging of functional connectivity in the developing brain during sleep using wearable high-density diffuse optical tomography

Julie Uchitel[a,b,*], Borja Blanco[a,c], Liam Collins-Jones[a], Andrea Edwards[d], Emma Porter[d], Kelle Pammenter[d], Jem Hebden[a], Robert J Cooper[a], Topun Austin[d]

[a] DOT-HUB, Department of Medical Physics and Biomedical Engineering, UCL, London, UK
[b] Department of Pediatrics, University of Cambridge, Cambridge, UK
[c] Department of Psychology, University of Cambridge, Cambridge, UK
[d] Neonatal Intensive Care Unit, Cambridge University Hospitals NHS Foundation Trust, Cambridge, UK

ARTICLE INFO

Keywords:
High-density diffuse optical tomography
HD-DOT
Cot-side neuroimaging
Newborn neuroimaging
Resting state functional connectivity
Functional connectivity
Newborn sleep states

ABSTRACT

Studies of cortical function in newborn infants in clinical settings are extremely challenging to undertake with traditional neuroimaging approaches. Partly in response to this challenge, functional near-infrared spectroscopy (fNIRS) has become an increasingly common clinical research tool but has significant limitations including a low spatial resolution and poor depth specificity. Moreover, the bulky optical fibres required in traditional fNIRS approaches present significant mechanical challenges, particularly for the study of vulnerable newborn infants. A new generation of wearable, modular, high-density diffuse optical tomography (HD-DOT) technologies has recently emerged that overcomes many of the limitations of traditional, fibre-based and low-density fNIRS measurements. Driven by the development of this new technology, we have undertaken the first cot-side study of newborn infants using wearable HD-DOT in a clinical setting. We use this technology to study functional brain connectivity (FC) in newborn infants during sleep and assess the effect of neonatal sleep states, active sleep (AS) and quiet sleep (QS), on resting state FC. Our results demonstrate that it is now possible to obtain high-quality functional images of the neonatal brain in the clinical setting with few constraints. Our results also suggest that sleep states differentially affect FC in the neonatal brain, consistent with prior reports.

1. Introduction

The investigation of resting state functional connectivity (RSFC) in newborn infants has significantly enriched our understanding of the intrinsic functional architecture of the developing brain. RSFC is inferred from the synchronized activity of different brain regions at rest, such that regions exhibiting higher temporal synchronization can define RSFC networks (Damoiseaux et al., 2006; Fransson et al., 2007). Among the many neuroimaging techniques, functional magnetic resonance imaging (fMRI) is typically used in these studies. In this, fMRI is sensitive to the blood-oxygen-level-dependent (BOLD) signal, which is associated with changes in concentration of deoxygenated haemoglobin and thus is a proxy for neuronal activity.

While fMRI offers many advantages, it is poorly suited for newborn infants in clinical settings. fMRI studies cannot be performed cot-side and require prolonged durations away from clinical units. fMRI also requires subjects to remain motionless for the duration of the recording, such that infants often need to be sedated (Arthurs et al., 2012). Sedation has also been shown to impact functional hyperaemia (Slupe and Kirsch, 2018). These conditions significantly limit the number and types of studies that can be performed in newborn infants, particularly for those that are vulnerable.

One area of growing interest in newborn functional brain imaging research is the impact of sleep on the developing brain. The emergence of sleep, sleep wake cycling, and sleep states in early life coincides with the emergence of functional networks in the brain. In newborn infants (neonates), sleep is typically divided into two states: active sleep (AS) and quiet sleep (QS). Electroencephalography (EEG) studies have found that these states demonstrate distinct functional connectivity (FC) network dynamics (Tokariev et al., 2019; Wielek et al.,

Abbreviations: High-density diffuse optical tomography, (HD-DOT); functional near infrared spectroscopy, (fNIRS); resting-state functional connectivity, (RSFC); functional connectivity, (FC); functional magnetic resonance imaging, (fMRI); oxygenated haemoglobin, (HbO); deoxygenated haemoglobin, (HbR); grey matter, (GM); connectome-based independent component analysis, (connICA); electroencephalography, (EEG); active sleep, (AS); quiet sleep, (QS); optical density, (OD); independent functional connectome components, (ICs).

* Corresponding author at: Department of Pediatrics, University of Cambridge, DOT-HUB, University College London, Cambridge, UK.
E-mail address: juchitel1@gmail.com (J. Uchitel).

https://doi.org/10.1016/j.neuroimage.2022.119784.
Available online 1 December 2022.
1053-8119/© 2023 The Authors. Published by Elsevier Inc. This is an open access article under the CC BY license (http://creativecommons.org/licenses/by/4.0/)

2019; Tokariev et al., 2016). Furthermore, abnormalities in sleep state dynamics and sleep wake cycling during the neonatal period are associated with altered neurodevelopmental outcomes in older infants (Shellhaas et al., 2017) and children (Stangenes et al., 2017). While EEG is highly applicable in clinical settings and can allow for long recordings, EEG is limited to cortical electrical activity, and cannot provide information on the haemodynamic changes that fMRI is sensitive to. EEG also has relatively poor spatial resolution, (Burle et al., 2015) and thus is limited in its capabilities to extract features of functional networks.

Functional near-infrared spectroscopy (fNIRS) surmounts many of these challenges by allowing for studies of cortical haemodynamic brain activity in a manner analogous to fMRI, but outside of the traditional brain imaging environment (Pinti et al., 2020). The standard fNIRS method uses arrays of optodes (sources and detectors of near-infrared light), sparsely distributed over the scalp to provide measures of haemodynamics in the underlying tissues. When compared with fMRI, fNIRS demonstrates higher temporal resolution, and has the advantage of being able to determine changes in the concentrations of both oxy- and deoxy-haemoglobin. However, the spatial resolution of typical fNIRS systems is on the order of 3 cm, significantly lower than fMRI (Scholkmann et al., 2014). Furthermore, the depth sensitivity of fNIRS is limited to the superficial cortex, (Quaresima et al., 2012) and typical arrangements of sources and detectors achieve little (if any) depth information, meaning changes in haemoglobin concentrations in the brain can be difficult to distinguish from those in the extracerebral tissues (Gagnon et al., 2012; Funane et al., 2014). Prior fNIRS studies investigating RSFC in newborn infants have demonstrated regional dependency and dynamic changes in interhemispheric FC within the first six months of life, (Homae et al., 2010) as well as altered FC patterns in preterm born neonates at term age (Fuchino et al., 2013; Naoi et al., 2013). A prior study used EEG-informed fNIRS analysis to assess FC across AS and QS in healthy newborns (Lee et al., 2020). However, this study had only a relatively small number of light sources and detectors available, which limited both the proportion of the cortex that could be interrogated and the spatial resolution of the resulting maps of underlying FC.

Diffuse optical tomography (DOT) is an evolution of fNIRS that permits the production of three-dimensional images of the optical properties of a target object (White and Culver, 2010). Measurements with a range of source-detector separations (known as channels) and spatially-overlapping sensitivity distributions are essential to DOT approaches (White and Culver, 2010). This necessitates detector technology with a very high dynamic range, and denser arrangements of source and detector optodes than are possible with standard fNIRS devices. In neonatal brain research in clinical settings, DOT studies have revealed RSFC networks in the visual cortex, (White et al., 2012). RSFC networks in the auditory cortex, (Ferradal et al., 2016) high-amplitude, biphasic pattern of changes concurrent with electrographic seizures, (Singh et al., 2014) and changes in interhemispheric FC following perinatal stroke (Chalia et al., 2019)

The concept of high-density diffuse optical tomography (HD-DOT) takes this concept one step further. In HD-DOT, an array of sources and detectors is employed that is dense enough to provide a continuous distribution of both short source-detector separation (~10 mm) channels and longer separation channels (spanning the 10–40 mm range) (White and Culver, 2010). This approach has been shown to significantly improve the disentanglement of extracerebral and cerebral haemodynamics in adults, (Funane et al., 2014) and has the capacity to yield cortical activation maps that approach the resolution of fMRI (Eggebrecht et al., 2014). Only one previous study has employed HD-DOT to study newborn infants in clinical settings (Liao et al., 2012). However, the technology used in that study, like most HD-DOT systems, required a large numbers of optical fibre bundles, compounding the mechanical challenge associated with studying newborn infant populations.

Recently, our group demonstrated a new generation of wearable HD-DOT systems. These modular, lightweight technologies allow for wide cortical coverage without sacrificing wearability, allowing for functional brain mapping to be undertaken outside of the traditional brain imaging environment (Vidal-Rosas et al., 2021). We have demonstrated the feasibility of using wearable HD-DOT approaches for retinotopic mapping of the adult visual cortex (Vidal-Rosas et al., 2021) and social stimuli response mapping in the infant (Frijia et al., 2021)

In the present study, we aimed to demonstrate that wearable HD-DOT can be adapted for use in newborn infants in clinical settings for cot-side studies of functional brain activity. As a secondary aim, we sought to demonstrate that this technology could be used to study features of FC during sleep and between neonatal sleep states.

2. Methods

2.1. Subjects

Healthy term-age neonates (born at ≥ 37 weeks of gestation) were recruited from the postnatal ward of The Rosie Hospital (Cambridge University Hospitals NHS Foundation Trust). This study was approved by the National Research Ethics Service Committee East of England (REC reference 15/LO/0358), and written informed consent was obtained from parents for neonates to participate. A total of 45 neonates were recruited. Datasets from 17 neonates were excluded during data processing due to insufficient duration of motion artifact-free data segments (described below) for subsequent FC analysis. HD-DOT data was analysed from the remaining 28 subjects (mean gestational age = 40 + 0 weeks (range: 38+2 – 42+1); mean weight at birth = 3522 g (range: 2890 – 4205 g); mean age at time of study = 3 days (range: 1–11 days). Demographic details of the subjects are summarized in Table 1.

2.2. Data collection

Cot-side data recording was performed on 45 neonates on the postnatal ward of The Rosie Hospital. To promote sleep, a feed and wrap approach was used. As a full-sleep cycle in the neonatal period typically lasts for up to an hour, (Scher, 2008) and we aimed to perform data recording sessions for one full hour. However, in certain cases of patients needing immediate clinical procedures or waking up before the end of the full hour, the study was ended early. If the infant was content to sleep for more than an hour, the infant was left undisturbed. Imaging session durations were on average 63.88 min (range: 34.60–144.77 min), Table 1. The HD-DOT system (cap, tiles, hub, cabling, and laptop, described below) and supporting equipment fit on a small trolley which was wheeled to the postnatal ward for studies. The setup also included video recording of behaviour for sleep and sleep state assessment as shown in Fig. 1. A summary of the data collection, pre-processing, and analysis pipeline is shown in Fig. 2.

2.3. Wearable HD-DOT system

We employed a wearable HD-DOT system known as LUMO (*Gowerlabs Ltd, UK*) (Vidal-Rosas et al., 2021; Frijia et al., 2021). The system consists of multiple independent modules (or "tiles", Fig. 1) that together create a dense network of sources and detectors, while still allowing the system to conform to the scalp. Each hexagonal sensor tile is equipped with 3 dual-wavelength LED sources (at 735, 850 nm) and 4 photodiode detectors. Each module weighs ~6 g and measures 29 mm across at the widest point. Within-tile measurements are obtained with source-detector separations of approximately 10 mm and 20 mm. Cross-tile measurements are acquired for all separations within an array but only channels up to ~45 mm separation are expected to yield acceptable signal quality. The modules are located into a chain of "docks" that are clipped into a flexible head cap. The docks provide power and data transfer, and can be positioned anywhere within the cap. The dock chain connects via a single flexible cable to a "hub", which itself connects via USB to a laptop. As shown in Fig. 3, a disposable rubber "light-guide"

Table 1
Subject demographics.

Subject Number	GA at birth (weeks)	Age (days)	Weight (g)	Recording Duration (min)	Sleep States Present (state and duration in min)
1	40 + 2	1	4035	52.02	QS = 3.13
2	40 + 4	1	3580	63.03	QS = 10.45
3	40 + 5	3	2890	46.08	QS = 18.37
4	41 + 5	8	3950	34.60	AS = 10.5
5	40 + 2	4	3885	144.77	QS = 29.42; AS = 20.88
6	41 + 5	2	3830	34.92	QS = 3.35
7	39 + 2	1	3385	60.72	QS = 5.02
8	41 + 1	4	4205	63.34	QS = 3.35; AS= 4.18
9	38 + 5	2	3530	71.18	QS = 3.28
10	39 + 3	6	3075	79.19	QS = 28.33; AS = 3.32
11	39 + 2	4	3275	50.04	AS = 4.30
12	40 + 3	4	3085	69.69	QS = 12.03; AS = 3.67
13	40 + 3	2	3840	61.32	QS = 3.52
14	41 + 0	4	4165	35.05	QS = 17.48; AS 3.97
15	39 + 5	5	2940	60.83	QS = 5.08
16	40 + 4	2	3275	64.11	QS = 6.62
17	39 + 0	5	3780	41.20	QS = 16.2
18	42 + 1	2	4150	69.25	QS = 4.23
19	39 + 0	1	3970	61.40	AS = 4.93
20	38 + 2	1	3170	75.27	QS = 3.37
21	39 + 6	1	3155	64.56	AS = 9.77
22	39 + 1	1	3570	72.88	QS = 9.45
23	41 + 0	2	3115	68.83	AS = 3.15
24	39 + 2	4	2910	64.99	QS = 10.6; AS = 6.57
25	39 + 4	1	3240	70.15	QS = 3.01;
26	40 + 5	2	3270	67.80	QS = 18.15;
27	39 + 0	11	4160	60.65	QS = 7.25
28	38 + 3	3	3185	75.30	QS = 11.163

containing seven short plastic optical fibres couples light through the dock to and from the scalp.

2.4. Neonatal HD-DOT Cap design

To form a complete cap, the LUMO dock chain was integrated into a neonatal EasyCap (Easycap GmbH, Germany). The EasyCap consists of a flexible cap made of elastane with a Velcro chin strap, and is commonly used for EEG studies (Fig. 3). This design was found to provide good optical coupling and efficient fitting (< 5 min). When compared to our prior study in 6-month-old infants that used LUMO with a more rigid cap made of neoprene and Velcro strapping, we found that newborn infants were generally more tolerant of the EasyCap material. Newborn infants also have more variable head shapes, which the more flexible material of the EasyCap material could better accommodate. The EasyCap has also been used in previous fNIRS studies with infants (Bulgarelli et al., 2020; Bulgarelli et al., 2019). Two caps were made to accommodate variable head circumferences (between 33.5 and 36 cm).

For this study, we designed a layout of 12 tiles and docks covering the frontal and parietal cortices. These 12 tiles provide 36 source locations, 48 detector locations and a total of 1728 channels per wavelength. Approximately 400 channels per hemisphere were expected to provide a source-detector separation below 45 mm and thus provide viable signals. Optode locations and the associated channels are illustrated in Fig. 4. This array design represents the equivalent of 84 optical fibres. The frame rate of this device was 10 Hz.

2.5. Cap positioning and spatial registration

The infant's head circumference was measured around the crown, and this distance was used to determine the correct cap size. The cap was placed on the infant's head and adjusted such that the front lip of the cap came down just over the eyebrows and the tiles were located over most of the frontal and parietal cortices. The cap design, positioning, and fit are shown in Figs. 1–4**a**.

For spatial registration of optode locations, we employed a three-dimensional structured illumination scanning approach as in our prior study of 4-7 month old infants (Frijia et al., 2021). For each participant, we acquired a three-dimensional model of the head surface using the TrueDepth camera functionality of an X-series iPhone (Apple, Inc., CA, USA) and the app ScandyPro (*Scandy LLC, USA*), which together allow scaled, 3D point clouds to be acquired and exported in a readily accessible format. As the inevitable movement of the infant, even during sleep, makes acquiring a continuous 360-degree scan nearly impossible, we acquired several depth-resolved 'snapshot' scans from different angles for each participant while the cap was in place. Each snapshot scan lasted approximately 1–8 s and was repeated if the baby moved during acquisition. The viewing angle of each snapshot was chosen to ensure at least three LUMO tiles and one cranial landmark were in the frame in each case and together the snapshots would cover both arrays, the nasion, inion, pre-auricular points and the vertex (Cz). The resulting multiple partial point clouds (see example shown in Fig. 4**b**) were then registered to one another using the software package CloudCompare (www.danielgm.net/cc), which uses equivalent point pairs that are manually identified across different partial scans to rigidly transform those partial point clouds to produce a complete model (Fig. 4**c**). To identify the exact location of sources and detectors, each tile was tagged with a specially designed fluorescent coloured triangular marker (Fig. 4**a** and **b**), the points of which were positioned directly above the sources of each tile. Because the tile and docks are of known dimensions, identifying the locations of the points of each triangle (Fig. 4**c)** provides sufficient information to determine the location of each optode location on the scalp without approximation. The location of subject-specific cranial landmarks (nasion, inion, pre-auricular points, Cz) and the position of each source and detector on the scalp could then be determined from the completed point cloud. A multi-layer neonatal tetrahedral head model was selected from a database of models (Collins-Jones et al., 2021). The head model was then registered to the space of each infant based on the affine transform between the cranial landmarks positions of the infant and the head model (Fig. 4**e**).

2.6. Sleep state assessment

The video recordings of infants were reviewed offline to classify the periods during which each infant was in one of two possible sleep states, AS or QS, for comparison of differences in FC between these two states

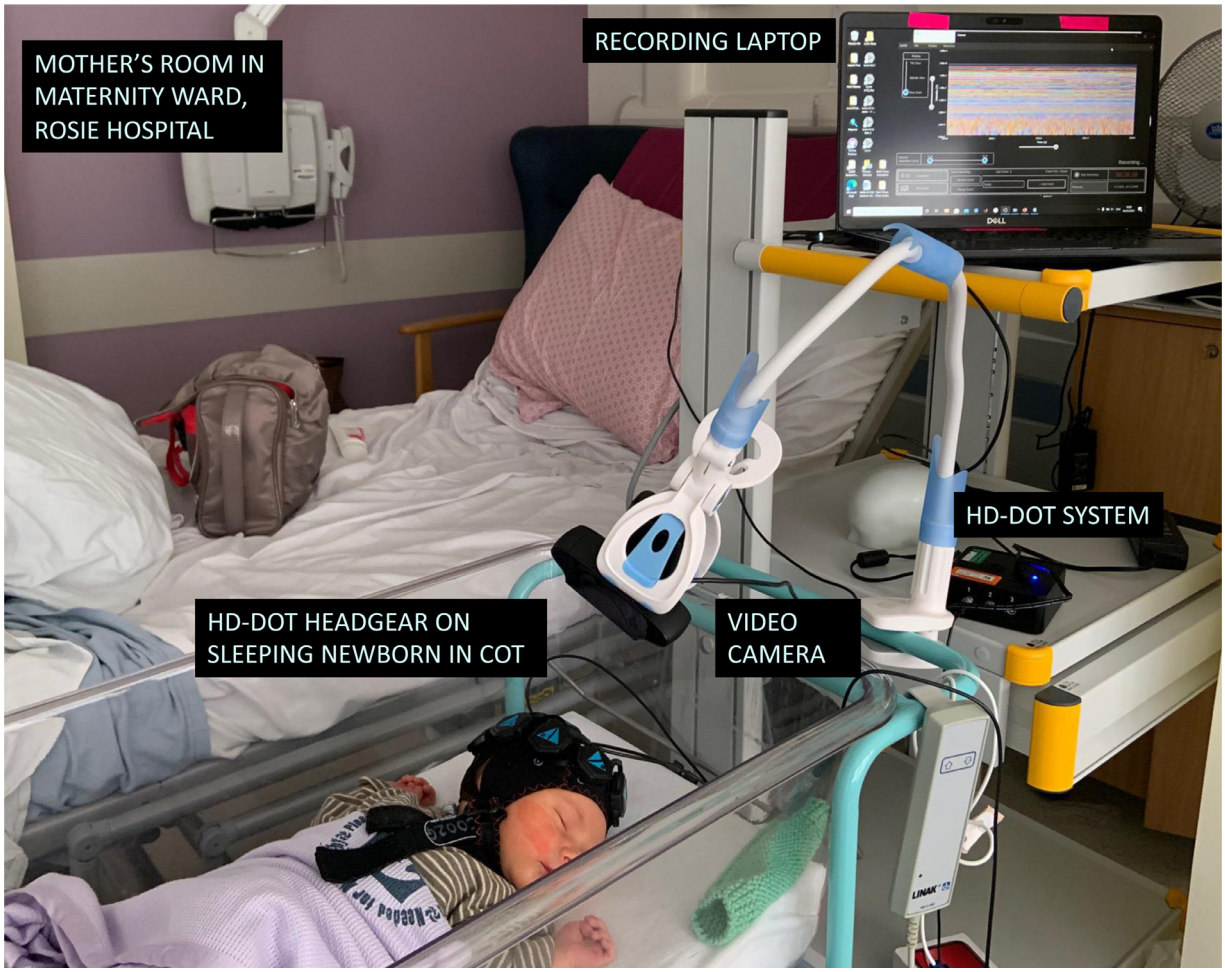

Fig. 1. *Functional Imaging of the Newborn Brain Cot-side*. Newborn infants were imaged cot-side in their mother's rooms in the maternity ward of the Rosie Hospital. All study materials fit on to a trolley that could be wheeled to the room. The HD-DOT cap was placed on the infant's head once they were asleep. The cap connects to a small control unit ('hub'), which transmits collected data to a laptop. A video camera was positioned above the infant for video recording of sleep state behaviours. Set up of all elements of this system took approximately 15 min.

as demonstrated in our prior study (Lee et al., 2020). Standard criteria for classifying neonatal sleep states based on behaviour was used (Scher, 2008; Dereymaeker et al., 2017; Hakamada et al., 1981). Video segments were classified as AS if the infant demonstrated a combination of two or more of the following behaviours: rapid eye movements, facial twitches, increased variability of respiration rates (visually assessed by chest movements), and frequent large body movements. Video segments were classified as QS if the infant demonstrated decreased variability in respiration rates, minimal facial movement, and minimal body movement except for occasional startle reflexes. Of note, given that the infant moves during AS, more motion artifact was observed during AS than QS. Example videos of the behavioural features of each state can be found in the **Supplementary Material**.

2.7. HD-DOT data pre-processing

In an initial assessment of the data, channels were discarded based on their coefficient of variation (rejected if mean of intensity/standard deviation of intensity ≤ 12). This coefficient of variation threshold was chosen based on the threshold used in our prior study using this HD-DOT system in adults (Vidal-Rosas et al., 2021) and the foundational RSFC study using HD-DOT in adults (White et al., 2009). Data segments with motion artifact were then excluded based on the channel-wise data using the hmrMotionArtifact function in the fNIRS data analysis toolbox *Homer2* (Huppert et al., 2009). Any change in measured optical density (OD) occurring within any 0.5 s period that was greater than 0.5 OD, or greater than 10 times the standard deviation of the entire time-course was considered to be motion artifact (parameters selected based on prior publications (Lee et al., 2020; Vidal-Rosas et al., 2021)). To minimize any potential impact of motion artifact on the surrounding data periods, 10 seconds of data before the start and after the end of each segment identified as motion artifact were also excluded.

Previously reported infant RSFC fNIRS studies have used a range of data recording durations for analysis: Bulgarelli et al (2019, 2020) employed a minimum of 100 seconds of resting state data comprised of individual segments at least 5 seconds in duration that were concatenated (Bulgarelli et al., 2020; Bulgarelli et al., 2019). Both Lee and Blanco et al (2020) and White et al (2012) used a minimum of 2 min of data (Lee et al., 2020, White et al., 2012). Wang et al (2017) used graph theory metrics to determine that FC could be accurately and stably achieved after 7.0 min fNIRS imaging duration at high network thresholds, whereas the necessary scanning time minimum was 2.5 min at low network thresholds (Wang et al., 2017) Blanco et al (2021) reported using ~9 min of data (Blanco et al., 2021).

Given this great variability, we chose to use 3 min of motion artifact-free data as our minimum. Thus, optical intensity data segments that were at least 3 min in length were extracted, and using the corresponding video, each segment was classified as AS or QS. From raw optical intensity data segments, changes in OD were calculated using the hmrIntensity2OD algorithm implemented in Homer2.[36] Motion artifact

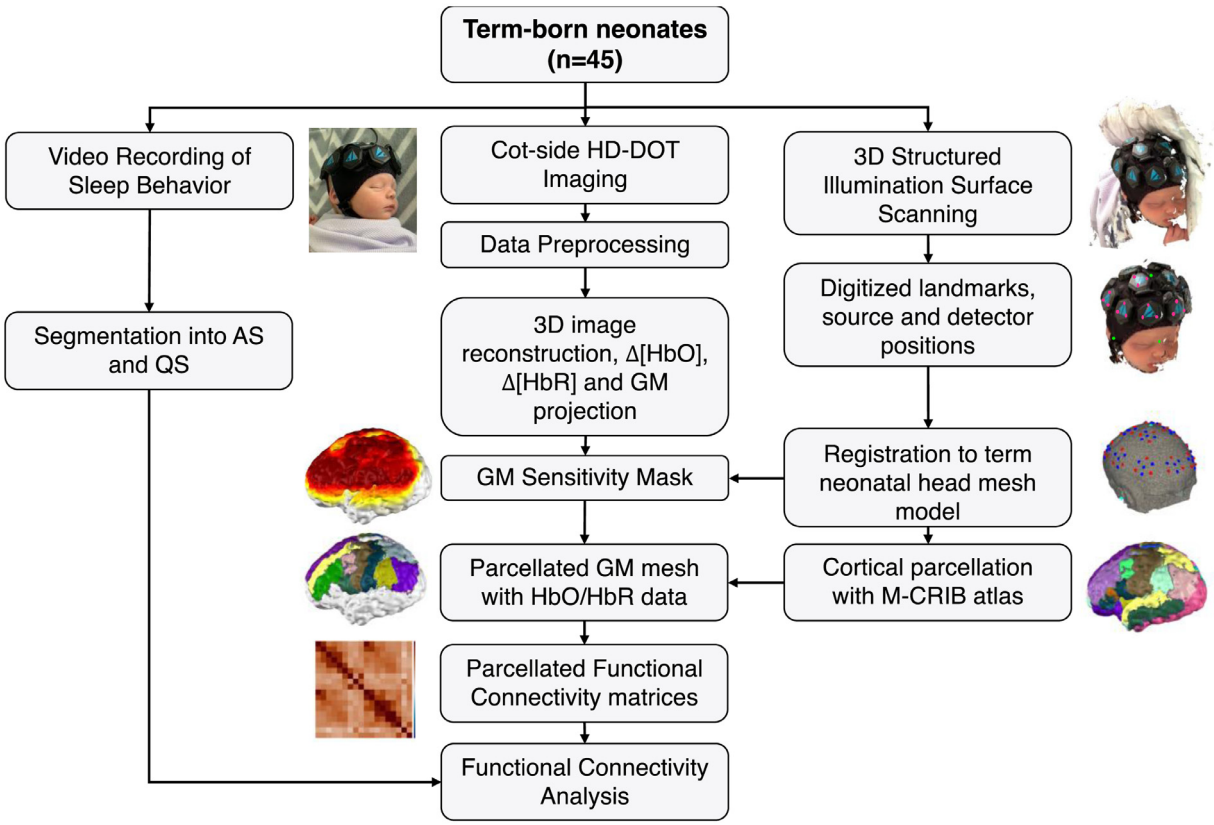

Fig. 2. *Project outline*. Summary of methods for data collection, data preprocessing, and higher-level functional connectivity analyses. AS (active sleep); QS (quiet sleep); HbO (oxygenated haemoglobin); HbR (deoxygenated haemoglobin); GM (grey matter).

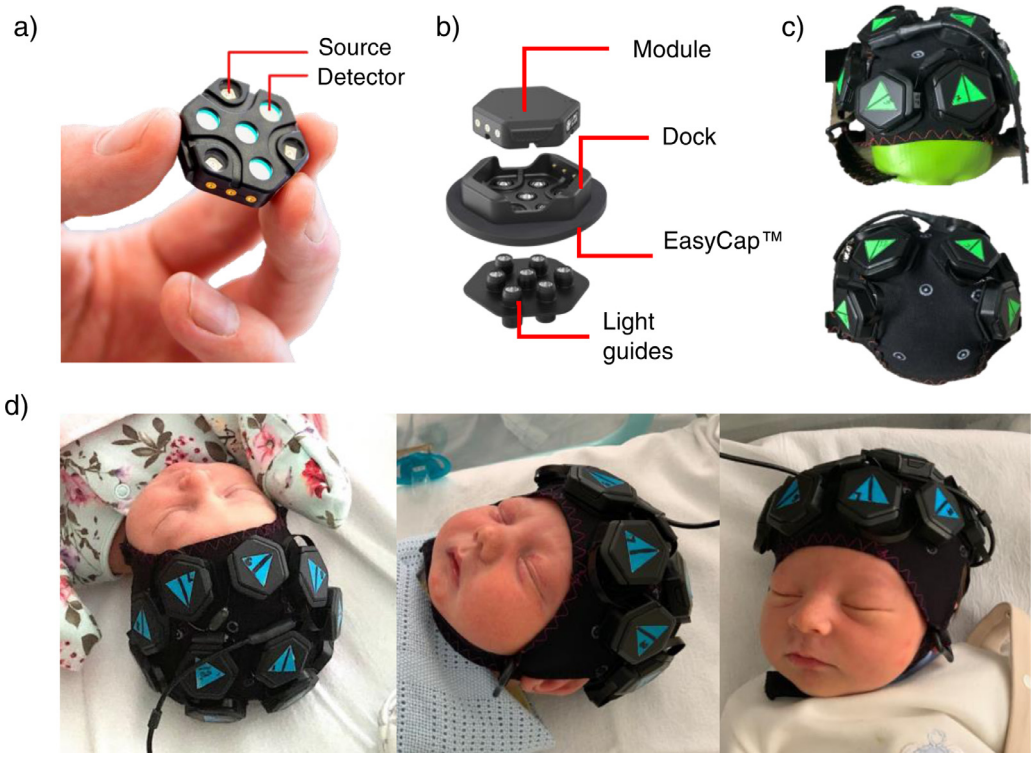

Fig. 3. **(a)** LUMO tile with source and detector positions indicated. **(b)** Positioning of docks into which the hexagonal tiles are located. The light-guide piece contains seven short optical fibres with length 4.5 mm. **(c)** Custom-designed neonatal HD-DOT cap containing 12 LUMO tiles. The 12 tiles and dock chain are integrated into an EasyCap. Front and back views of the cap are shown. **(d)** Photographs of the cap on three newborn infants during cot-side data recording with tiles visible over the frontal and parietal cortices.

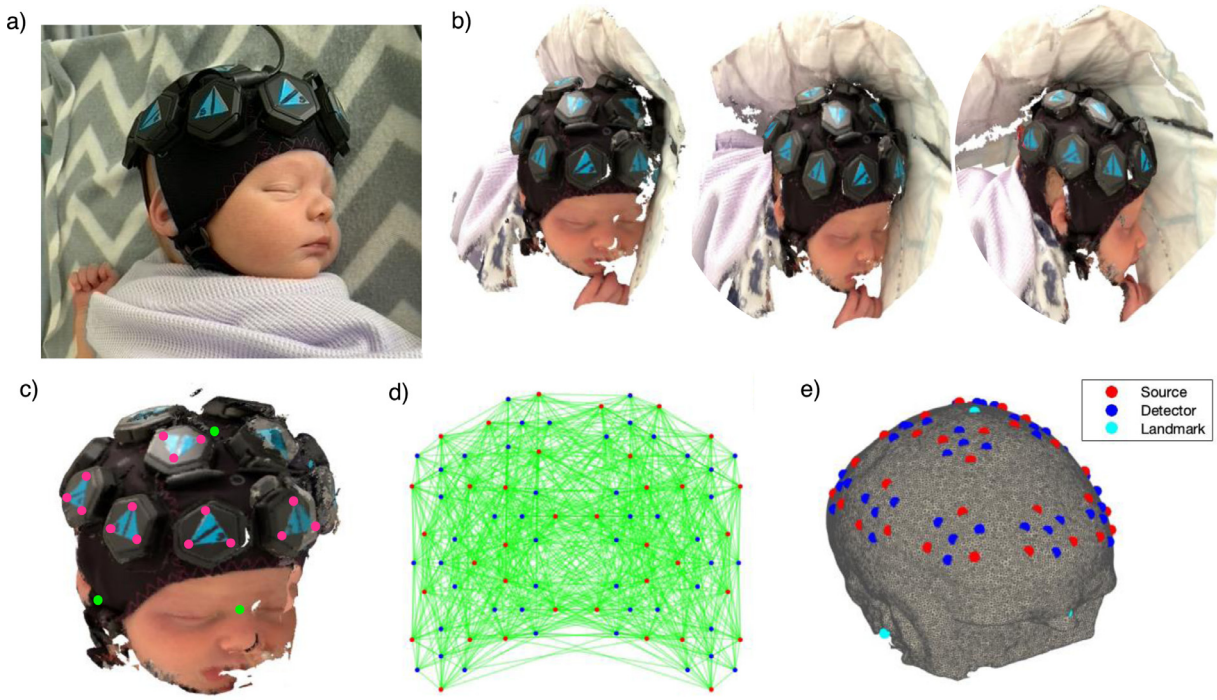

Fig. 4. **(a)** A photograph of a newborn infant in their cot wearing the HD-DOT system. **(b)** Three snapshot point cloud images of an infant. **(c)** The complete model for that infant, created from multiple point cloud images with cranial landmarks (green points) and sources marker locations (magenta points). (**d)** A 2D representation of the full 12 tile array showing channels with source–detector separation of approximately ≤ 60mm in the 3D space. (**e)** The source positions (red points) and detector positions (blue points) shown on the shown on the scalp surface of the multi-layer neonatal tetrahedral head model registered to the subject's space.

correction was not used here as the effects of these techniques on temporal correlation are not well understood and have the potential to produce spurious network measures (Di Lorenzo et al., 2019). Instead, a more conservative approach of selecting only motion artifact-free data was implemented. In the case of infants that had more than one segment of the same sleep state (i.e. in the case of two segments of clean data at least 3 min in duration separated by a period of motion artifact), these segments were converted to OD and then concatenated, as studies suggests that concatenating RSFC time series of the same brain state (here, AS or QS) yields high reliability (Cho et al., 2021). The outcome was that 11 subjects had clean data segments classified as AS, and 23 subjects had data segments classified as QS, with 5 subjects yielding segments for both states (Table 1). The average time series of all short channels, which are primarily sensitive to scalp haemodynamics (Gregg 2010; Saager and Berger, 2008), were then regressed, as performed previously (Sato et al., 2016). Temporal filtering was then applied using a regression model (Caballero-Gaudes and Reynolds, 2017). Sine and cosine functions for frequencies above 0.08 Hz were included in the model to remove the contribution of physiological noise sources (e.g. respiration and cardiac pulsation), and up to 9th order Legendre polynomials (depending on dataset duration) were included to account for fluctuations at very low frequencies. The order was calculated as k = 1 + floor(length of data in seconds/150), where the shortest data segment was 181 seconds and the longest was 1153 seconds.

2.8. Image reconstruction

Images were reconstructed from the acquired data using a linear approach described previously (Arridge, 1999, Arridge and Schotland, 2009) The forward problem was modelled using the diffusion approximation (Arridge, 1999) The Jacobian matrix was calculated using Toast++ (Schweiger and Arridge, 2014) via the finite element method. The optical properties of the tissue layers of the model at the wavelengths of interest were linearly interpolated from literature values for each tissue (Bevilacqua et al., 1999). The Jacobian was calculated in a fine regular grid with size $30 \times 30 \times 30$ voxels and projected into a multi-layer neonatal tetrahedral head mesh for each infant (Schweiger and Arridge, 2003). The neonatal head model used in this study was selected from a neonatal head model database (Collins-Jones et al., 2021) whose head circumference was nearest to 34 cm, the average head circumference for this dataset. To determine the optical properties for each tissue at each wavelength, a regression was fit linearly to the values for the absorption and reduced scattering coefficients from three studies (Bevilacqua et al., 1999, Strangman et al., 2003, Ferradal, 2014). The values in the table below were taken was the values of the regression lines for each tissue at 735 and 850 nm. The optical properties associated with the tissue layers of this head model are presented in **Supplementary Table 1**. The changes in absorption coefficient were calculated via inversion of the forward model using zeroth-order Tikhonov regularization. The recovered images of the changes in absorption coefficient at the two wavelengths were then converted to images of changes in HbO and HbR concentrations (Cope, 1991). For visualization and further analysis, these haemoglobin images were then mapped from the tetrahedral volume mesh to the GM surface mesh of the head model.

A sensitivity map of the channel layout was then calculated in the GM space by finding a sensitivity mask for each subject. To create a sensitivity mask for each subject, we set a threshold of 5% of the maximum value of the normalized Jacobian such that nodes exhibiting a sensitivity above this value were set equal to 1 in a binary mask. All sessions' binarized masks were then summed to compute a group-level mask, such that if all subjects' masks were sensitive to a given node, the node value was 28. All nodes which had a value of 21 (75% of subjects) or above were included in the final group-level mask.

2.9. Parcellation of the cortical surface

Computing HbO and HbR FC matrices based on tens of thousands of GM surface mesh nodes is highly computationally expensive. To reduce

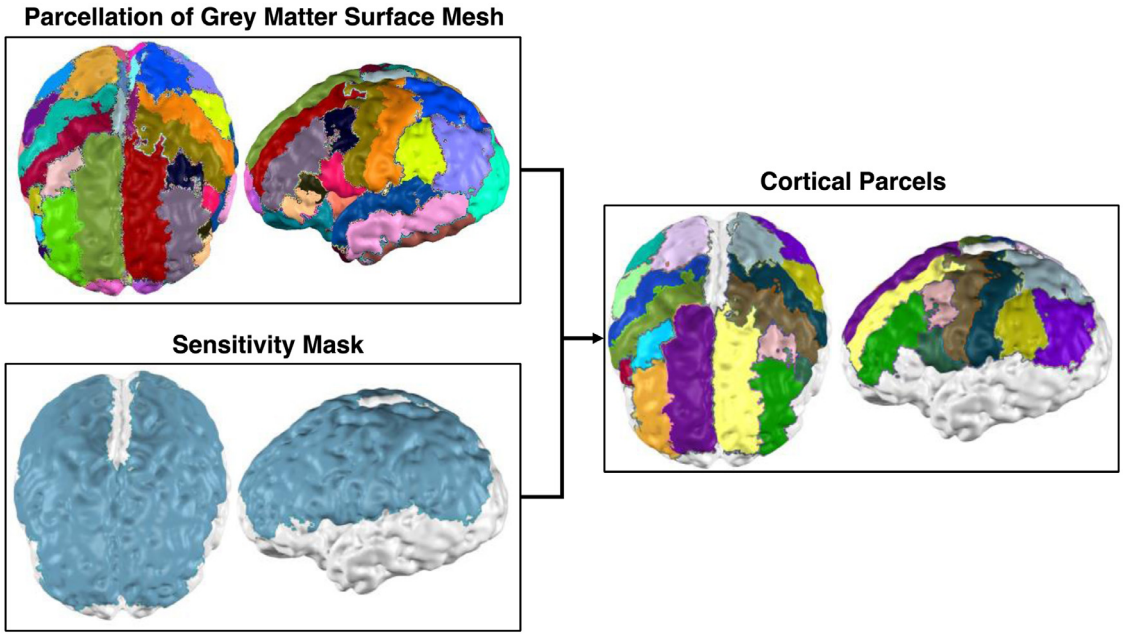

Fig. 5. *Cortical Parcellation to Reduce Data Dimensionality*. The GM surface mesh of the neonatal head model was parcellated according to the M-CRIB parcellation scheme. This was combined with the binary sensitivity mask of the 12-module array to produce an image of the cortical parcels that our system was sensitive to.

data dimensionality, a cortical parcellation approach was used. This approach also provides the benefit of indicating which nodes correspond to which anatomical brain regions. In this approach, the GM surface mesh is divided into parcels and the HbO and HbR values for all nodes within each parcel are averaged to produce a single HbO and HbR value for each parcel at each time point.

Employing the approach detailed by Blesa et al. (2021) the M-CRIB atlas was used to parcellate the brain of the neonatal head model. The M-CRIB atlas was chosen as compared to other atlases as it is based on both anatomical and functional information. The M-CRIB atlas consists of 10 neonatal subjects whose MRI volumes have undergone manual neuroanatomical labelling (Alexander et al., 2019). Using the developing Human Connectome Project processing pipeline (Makropoulos et al., 2018; Makropoulos et al., 2014), the T_2-weighted intensity images of all 10 atlas individuals included in the M-CRIB 2.0 release were processed to obtain a brain mask and tissue segmentations. These brain masks and segmentations were used to perform histogram matching between the T_2-weighted volumes of each M-CRIB atlas and the database-chosen model. Each of the M-CRIB T_2-weighted volumes were then non-linearly registered to the T_2-weighted volume of the database-chosen model using the SyN function of the ANTS toolbox; (Avants et al., 2008) this transform was used to register the manual labels of each M-CRIB volume to the space of the multi-layer neonatal tetrahedral head mesh. These registered labels were then merged using a joint label fusion approach as detailed by Wang et al. (2013). The output of this process was a parcellation of 84 regions of interest within the space of the neonatal head model.

The group-level sensitivity mask was then applied to the GM surface mesh of the parcellated head model, producing a map of parcels that the array was sensitive to (Fig. 5). Parcels were included if the array was sensitive to at least 50% of the GM surface mesh nodes belonging to that parcel (as determined by the GM sensitivity mask, see above) and across at least 75% of the subjects (21/28 subjects, 75%). Once the sensitivity profile of the system was applied to the parcellated cortex, 18 parcels remained within the field-of-view of our experiment (Fig. 5). These parcels corresponded to the following regions: caudal middle frontal gyrus, inferior parietal gyrus, pars opercularis, post central gyrus, precentral gyrus, rostral middle frontal gyrus, superior frontal gyrus, superior parietal gyrus, and supramarginal gyrus (for right and left, n=18 total). This parcellation was applied to each subject's data to produce FC matrices of size 18 × 18. Group-level FC matrices were produced by averaging all subjects' parcel-space FC matrices.

2.10. Functional connectivity analyses

2.10.1. Seed based correlation

As an initial validation that FC was present in this dataset and that physiologically meaningful FC maps could be demonstrated, a seed-based correlation analysis was employed. This analysis used the longest data segment for each subject, regardless of sleep state (i.e. if a subject had both AS and QS data segments, whichever segment was longer in duration was included). Hereafter, these data segments are referred to as 'all subject data'. In the GM mesh space, seed regions of 3.5 mm radius for the left and right hemispheres were selected for the prefrontal, motor, and parietal regions based on previously published reports (Ferradal et al., 2016; Doria et al., 2010; Smyser et al., 2010) and the anatomical locations of these regions on the GM surface mesh (e.g. in the centre of the prefrontal gyrus/motor cortex). Within this seed region, the average of all nodes' HbO and HbR signals was calculated, and this averaged signal was the 'seed' signal. Then, a robust Pearson's correlation coefficient (Santosa et al., 2017) was calculated between each seed signal and the signal of every other node in the GM surface mesh that fell within the GM sensitivity mask. Robust correlation was performed to minimize the impact of outlier timepoints for correlation analysis (Santosa et al., 2017). Individual correlation values were normalized by Fisher's Z transformation before averaging across subjects. *Z*-transformed maps were converted to t-statistics and thresholded with FDR correction to 0.005.

2.10.2. Cortical parcel connectivity analysis

In order to further investigate the presence of FC in this dataset, we analysed the temporal correlations of the continuous HbO and HbR signals for four different types of connectivity (Imai et al., 2014). For each infant's parcellated data, we calculated the correlation coefficients (r) between the HbO and HbR values of each of the 18 parcels. There were $(18 \times 18)/2 = 162$ parcel pairs and 162 r values were collected for each infant. Each r value was converted to a z-score by Fisher's *Z* transformation, and Z scores were averaged together to produce a single FC

value. Connectivity was categorized into the 4 following types: (i) short-range connectivity (26 pairs), (ii) contralateral transverse (interhemispheric) connectivity (30 pairs), (iii) ipsilateral-longitudinal connectivity (27 pairs), and (iv) control (70 pairs). Short range connectivity (i) was defined as parcels that were immediately anatomically adjacent to one another. Interhemispheric connectivity (ii) was defined as the connections between parcels that were contralaterally homologous (symmetric across the midline), or contralaterally homologous and one parcel over (i.e., left motor cortex and right motor cortex, left motor cortex and right somatosensory cortex). Ipsilateral-longitudinal connectivity (iii) was defined as connections in which each parcel in the pair was more than three parcels away from one another, which mainly comprised fronto-parietal connections. Control connectivity (iv) consisted of connections other than those of (i), (ii), and (iii). Overall connectivity was defined as all possible parcel pairings. The strength of each type of connectivity was evaluated by averaging the Z scores within the defined connectivity for each infant. Then, we obtained an averaged value of the Z scores for each type of connectivity for each group. Each of the four types of connectivity were statistically compared between one another and between sleep states using an independent t-test.

2.10.3. Connectome-based independent component analysis (connICA)

We assessed for the presence of specific FC networks using connectome-based independent component analysis (connICA), (Amico et al., 2017) a data-driven methodology based on independent component analysis. connICA can be used to extract group-level independent FC patterns from a set of individual FC matrices. This approach was chosen because it relies on the FC matrices of subject datasets, rather than time series, thereby overcoming the limitation of having different durations of data segments across subjects. In this approach, the upper triangle of the symmetric FC matrices of HbO and HbR is first vectorized for each subject. These vectors were concatenated in rows to form a group-level FC matrix of dimensions [11 AS subjects + 23 QS subjects] x [18 parcel pairs x 2 Hb chromophores]. The integration of the information on FC provided by HbO and HbR was done under the premise that similar FC patterns should be observed across chromophores (Ferradal et al., 2016; Mesquita et al., 2010; Homae et al., 2011). Next, the FastICA algorithm (Hyvärinen and Oja, 2000) was applied to this group-level matrix to obtain a set of latent group-level independent functional connectome components (ICs), and their corresponding weights in each infant. From this analysis 12 ICs were extracted, a number that is equal to the number of principal components necessary to explain 65% of the group data variance. The criteria for ICA model order selection are explained in detail in **Appendix 1**. Each IC has an associated set of 34 weights: 11 for AS subjects and 23 for QS subjects. Independent t-tests were used to compare the contributions of AS and QS weights to a given IC and its associated spatial map.

3. Results

3.1. Group-level functional connectivity matrices

Fig. 6 presents the group-level FC matrices for HbO and HbR with parcels ordered according to their anatomical location on the cortex, ordered from most anterior to most posterior. High correlation values near the diagonal indicate that anatomically adjacent parcels are most strongly correlated with one another (blue arrows). Correlation between contralateral homologous regions for parcels within the frontal cortex are also evident (dashed yellow boxes and arrows).

3.2. Seed based correlation

Fig. 7 presents the seed-based correlation maps for seeds in the left and right motor cortex, parietal cortex, and frontal cortex. Motor cortex maps show expected correlation down the length of the motor cortex outside and areas of the somatosensory cortex. Significant correlation is also seen on the motor cortex contralateral to the seed region. These effects are slightly more evident for the left seed than for the right and for HbO than for HbR. Parietal cortex maps show correlation in the parietal cortex surrounding the seed region, as well as in the contralateral parietal cortex. Notably, strong correlation is also seen in the frontal cortex, particularly for the right parietal seed, suggestive of fronto-parietal networks. Frontal cortex maps show the strongest correlation in the region immediately surrounding the seed region, as well as the contralateral equivalent portion of the frontal cortex. Correlation decreases radially

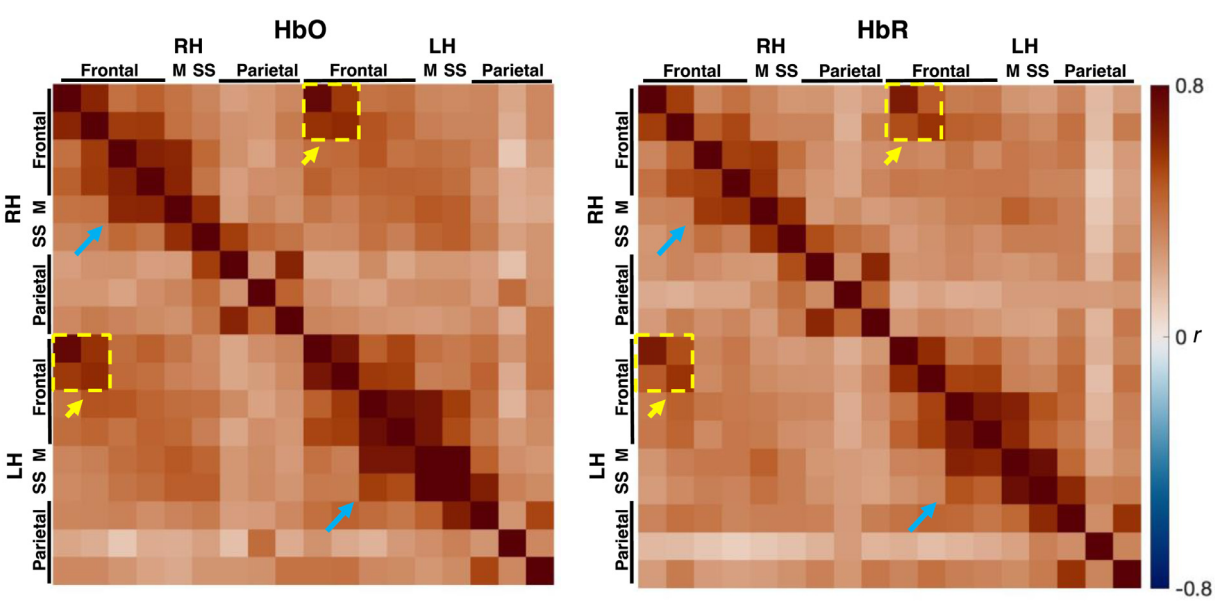

Fig. 6. *Group-level FC matrices.* Parcels are organized according to their anatomical location (from most anterior to most posterior) and divided into left (LH) and right (RH) hemispheres for HbO (left) and HbR (right). Dashed yellow squares and yellow arrows indicate apparent functional connectivity between contralateral homologous frontal regions. Blue arrows indicate off diagonal effects and strong correlations between anatomically adjacent regions. M (motor cortex parcel); SS (somatosensory cortex parcel).

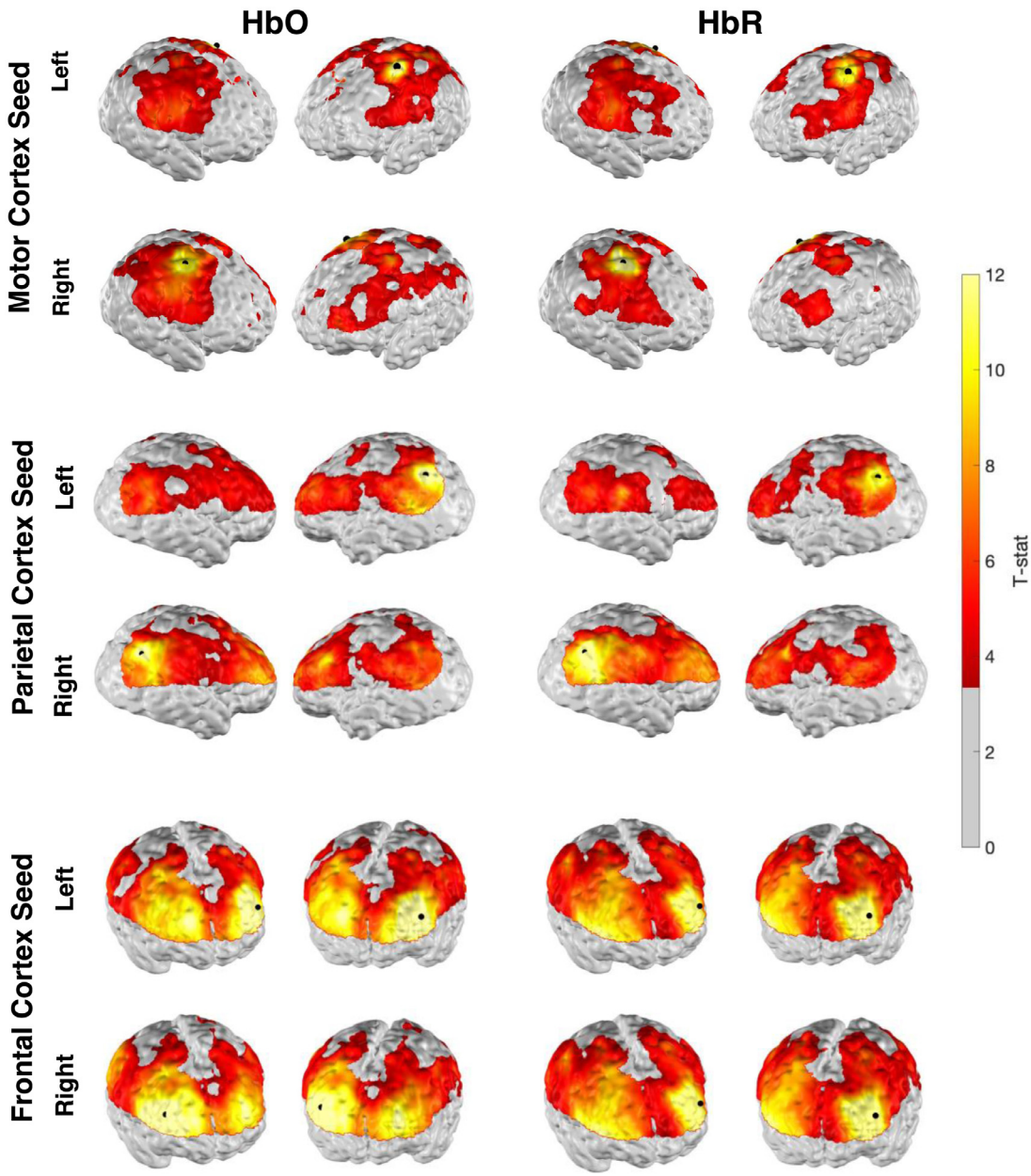

Fig. 7. *Seed based correlation analysis.* Seed based correlation maps for all subjects generated from seeds in the left and right motor cortex (top two rows), parietal cortex (middle two rows), and frontal cortex (bottom two rows) in the nodal space for HbO (left two columns) and HbR (right two columns). The seed region is displayed as a black point. Brighter yellow colours indicate more significant correlations between nodes and the seed region. Features of FC (correlation between contralateral brain regions, fronto-parietal correlations) are evident in these maps. Colorbar is thresholded in grey to the t-stat value corresponding to an FDR correction of 0.005.

on the cortex moving away from the frontal cortex towards more posterior regions, until reaching the parietal cortex, in which correlation increases, again supporting the presence of fronto-parietal networks. Altogether, these seed-based correlation maps appear to demonstrate physiologically meaningful FC patterns and the presence of expected FC networks.

3.3. Cortical parcel connectivity analysis

Fig. 8 presents the results of comparing connectivity strength when parcel pairs are classified into different connectivity types: short range, interhemispheric, longitudinal ipsilateral, or control. Considering all subjects, and as expected, short-range connections were significantly stronger than interhemispheric, longitudinal ipsilateral, and control connections for HbO and HbR ($p < 0.005$). Interhemispheric connections were also stronger than ipsilateral longitudinal and control for HbO ($p < 0.005$), and control only for HbR ($p < 0.005$). Considering subjects who had QS data, short-range connections were significantly stronger for all other types of connections for HbO and HbR ($p < 0.005$). No significant differences were found for connections during AS ($p = 0.0250$–0.9597 for HbO; $p = 0.0589$–0.9129 for HbR). No significant differences were found when connection types were compared between sleep states for any types of connections ($p = 0.1470$–0.9997 for HbO, $p = 0.2093$–0.6484 for HbR). The finding of higher FC values for interhemispheric connections than control connections supports the finding of the seed-based correlation analysis of significant FC between contralateral homotopic brain regions.

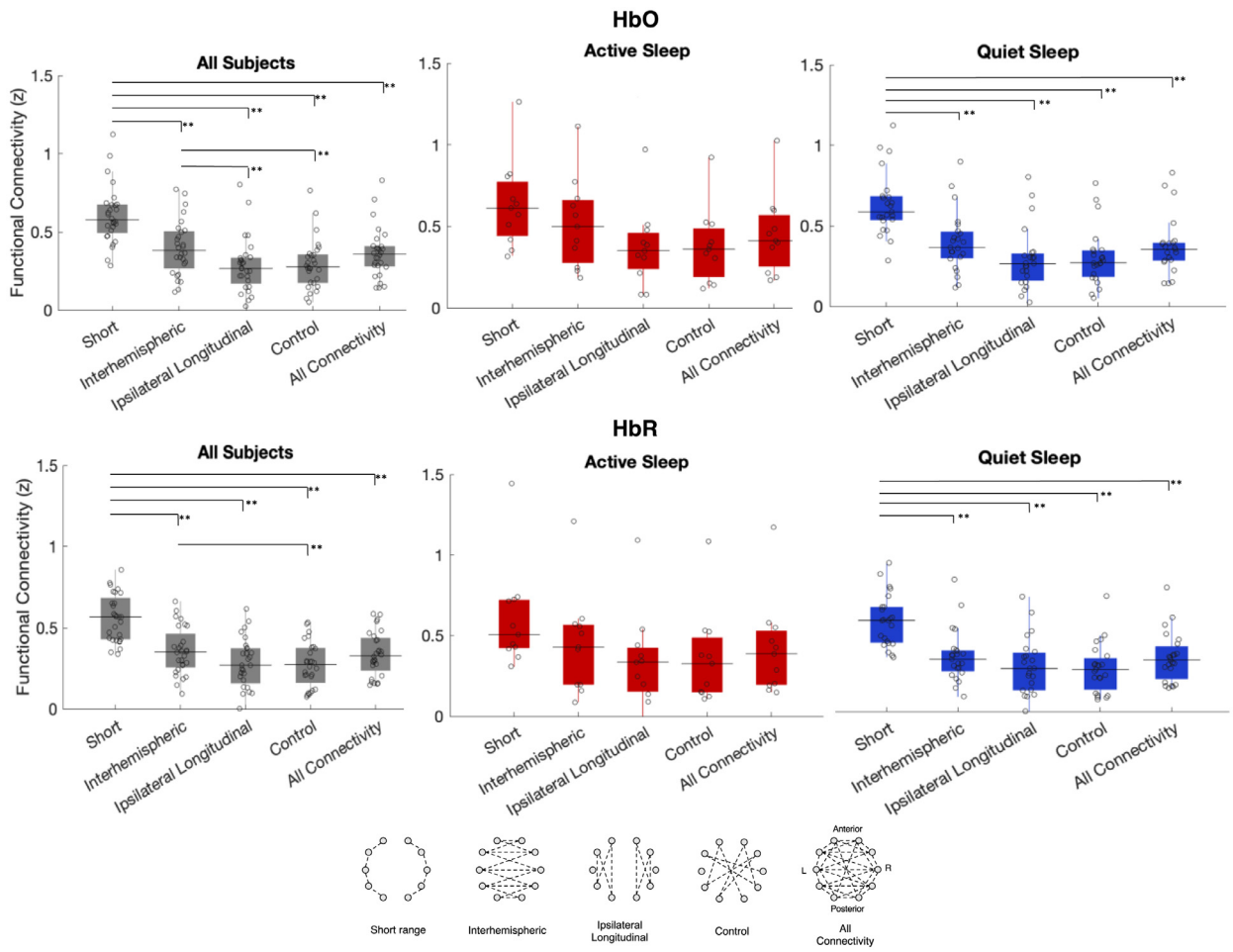

Fig. 8. *Cortical Parcel Connectivity*. Robust correlation values and *Z*-scores were calculated between all parcel pairs. Parcel pairs were then divided into groups according to type of connection: short-range, contralateral transverse/interhemispheric, ipsilateral longitudinal, or control. These are displayed below the box plots, grey circles represent parcels, dashed lines represent connections between parcels. Top row, HbO; bottom row, HbR. First column, all subjects' data, defined as the longest data segment for each subject independent of sleep state; second column, AS data segments; third column, QS data segments. FC, defined here as the averaged Z-score values for each type of connection, are plotted as open circles. FC was strongest for short-range and interhemispheric connections and weakest for ipsilateral longitudinal and control connections. $^{*}p < 0.05$, $^{**}p < 0.005$.

3.4. Connectivity-based independent component analysis (connICA)

Further evidence of the presence of FC, as well as modulation of FC resulting from variations in sleep state, was demonstrated by connICA (Fig. 9). As described above in the methods, the output of the connICA analysis is a set of ICs for the selected PCA threshold. Each IC corresponds to a spatial map demonstrating connections between nodes, where each node corresponds to the centre of a particular cortical parcel. Therefore, a connection between nodes represents a connection between two cortical parcels. In this analysis, 7 ICs were identified, each with an associated spatial map comprised of nodes and connections between nodes. The 7 spatial maps were visually evaluated to determine whether the spatial map demonstrated features of FC, i.e., that that resembled previously demonstrated FC networks or physiologically plausible connections within the brain. Of the 7, 5 demonstrated features that resembled previously demonstrated FC networks or physiologically plausible connections within the brain. These 5 are presented in Fig. 9, the remaining 2 maps not suggestive of any physiological patterns are presented in **Supplementary Fig. 2**.

The spatial map of one IC suggested FC patterns of interhemispheric connectivity (Fig. 9**a**) Weights for AS subjects in this network were significantly higher than weights for QS subjects, suggesting that this network is more present during AS than QS. Of note, this finding of stronger interhemispheric connectivity during AS is consistent with our prior study of differences between AS and QS in neonates using fNIRS (Lee et al., 2020). Among the other four selected ICs, notable FC patterns included frontal connectivity (Fig. 9**b**), right hemisphere intrahemispheric connectivity (Fig. 9**c**), left hemisphere intrahemispheric connectivity (Fig. 9**d**), and short-range local connectivity (Fig. 9**e**). For these spatial maps, no significant differences were observed in the weights of AS and QS ($p = 0.114$–0.862).

4. Discussion

To our knowledge this is the first study to employ wearable HD-DOT in the newborn infant for cot-side neuroimaging. We adapted a previously demonstrated HD-DOT technology to the neonatal population through the development of a newborn-friendly headgear that allowed for long recording durations. We used this system to perform cot-side studies of functional brain activity during sleep and compare FC dynamics across newborn infant sleep states, AS and QS. Our findings demonstrate the feasibility of performing studies in newborn infants in clinical settings using wearable HD-DOT, and particularly to characterize task free, or resting-state (here, sleep) FC networks in the brain.

The fibreless, modular, and portable design of the system employed in this study enabled the application of a large number of sources and detectors to the head with minimal preparation or disturbance to newborn infants. All of our study equipment could be easily transported on a

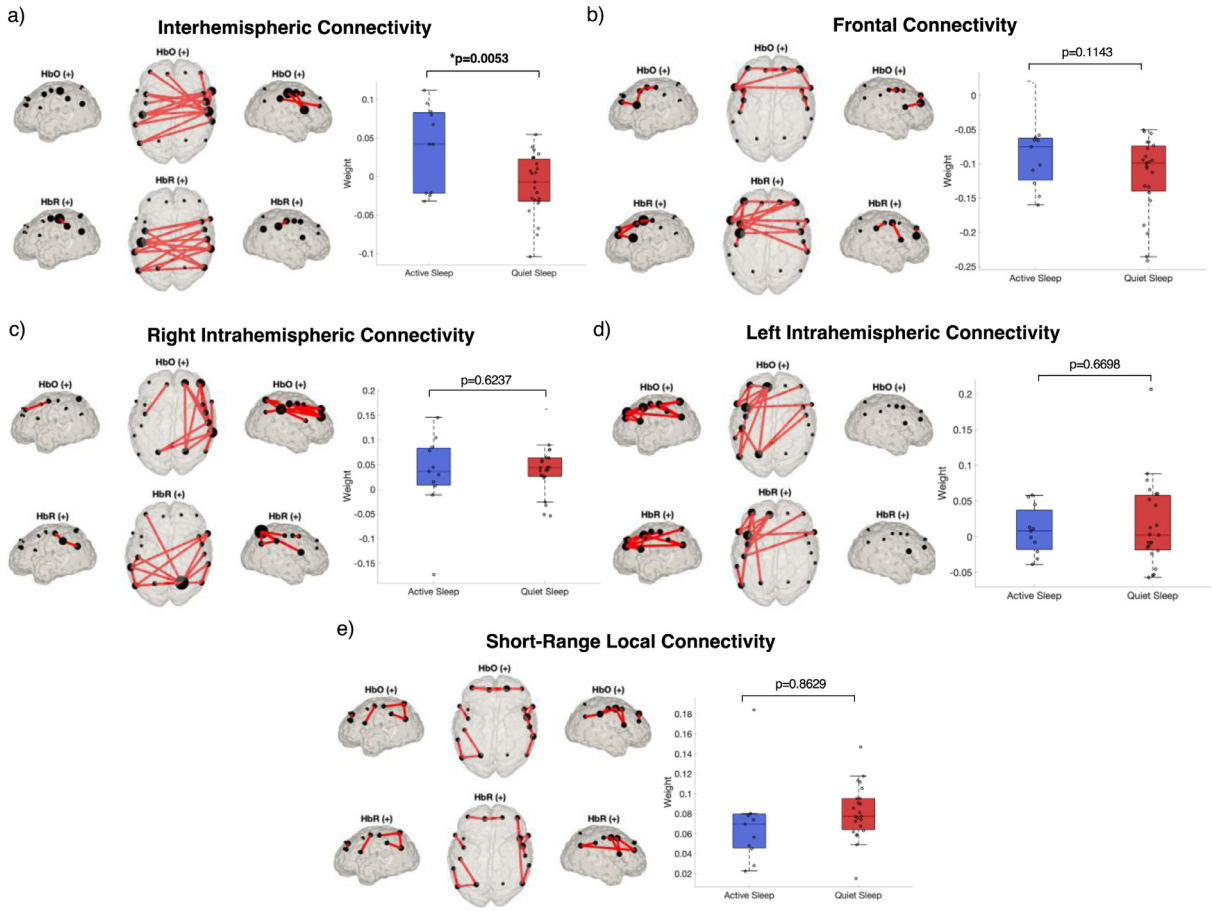

Fig. 9. *Results of connICA analysis*. Five spatial maps demonstrating patterns suggestive of FC were identified. These patterns include interhemispheric connectivity, frontal connectivity, right hemisphere intrahemispheric connectivity, left hemisphere intrahemispheric connectivity, and short-range local connectivity. Each node in the spatial map corresponds to the centre of a particular cortical parcel, and connections between nodes represent functional connections between parcels. The spatial map in a) represents a FC pattern formed by interhemispheric edges showing a higher prominence during AS than QS (p = 0.0053).

trolley such that the infant could remain in a naturalistic setting in their cot next to their mother during the study. The total time from the trolley entering the mother's room on the postnatal ward to the beginning of a recording was approximately 15 min. The system was well tolerated by the infants, and for long durations, with the maximum study duration lasting over two hours. These considerations are particularly important for vulnerable newborn infants, such as premature infants in intensive care, for whom bulky optical fibres or transport out of the intensive care unit is not feasible.

This study also represents the first application of a cortical parcellation scheme to 3D reconstructed HD-DOT data for newborn infants. This was performed to reduce the dimensionality of the data (from thousands of GM surface mesh nodes to 18 cortical parcels) to facilitate FC matrix generation and FC analyses. Cortical parcellation schemes have been previously used in fMRI studies of adults (Lewis et al., 2022; Gordon et al., 2016; Schaefer et al., 2018) and infants (Shi et al., 2018; Fenchel et al., 2020; Alexander et al., 2017) for similar purposes.

Our infant-friendly registration method enabled us to obtain the three-dimensional position of tiles relative to the cranial landmarks using the TrueDepth functionality of an X-series iPhone. Note that other devices, including the structure.io scanner (https://structure.io), are available to perform similar structured-illumination scanning.

Our FC analyses considering all subject data demonstrated strong evidence of FC networks present in our dataset. Group-level FC matrices demonstrated features of stronger correlation between anatomically adjacent regions, and stronger correlations between contralateral frontal regions. The seed-based correlation analyses revealed the expected homotopic correlation along the length of the motor cortices for the motor seeds. The expected fronto-parietal FC was also observed in the frontal seed and parietal seed correlations. Our connICA analysis produced 7 IC spatial maps, 5 of which were consistent with known patterns of FC and known FC networks (intrahemispheric connectivity, interhemispheric connectivity, short-range connectivity, and frontal connectivity).

Our sleep state analyses comparing FC network features across AS and QS demonstrated stronger interhemispheric connections during AS relative to QS, and stronger local, short-range connections during QS relative to AS. This was first demonstrated in our cortical connectivity analysis, in which QS had significant differences between the strength of short-range connections and all other types of connections (interhemispheric, longitudinal ipsilateral, control, all connectivity) (Fig. 8). This predominance of short-range connectivity was not observed for AS. Similarly, our connICA analysis revealed a spatial map with interhemispheric connections that more strongly represented during AS than QS (Fig. 9, p = 0.0053). These findings are consistent with our prior study using fNIRS in which network-based statistics and connICA analyses demonstrated stronger interhemispheric connections during AS than QS (Lee et al., 2020). In full-term neonates, more than half of sleep time is spent in AS (Mirmiran et al., 2003). Animal studies demonstrate that cerebral blood flow and oxygen delivery is relatively higher in AS compared to QS, (Morrison et al., 2005) and that cerebral metabolic rate of oxygen consumption is as high in AS as during wakefulness (Silvani et al., 2006). Alongside this evidence, the increased strength of interhemispheric connections during AS observed in this study suggest that AS may be

functionally important in early development for interhemispheric connections.

The ability to study FC in neonates at the cot-side has the potential to become a valuable clinical tool to assess cerebral function and development in vulnerable neonatal patients. This is of clinical importance as the incidence of neurodisability remains unchanged despite advances in neonatal care and improvements in survival rates (Costeloe et al., 2012). However, a number of issues must be addressed to yield more robust datatypes. Even with wearable technologies, it remains difficult to capture a continuous recording of sufficient length that is motion artifact-free in neonates. This was one of the main limitations of this work. It is even more challenging if limited to a specific sleep state, and greater still if there are segments of sleep states that are not easily identifiable as AS or QS. As a result of these requirements, the durations of remaining data will inevitably be shorter than is desirable. Previous fNIRS RSFC studies reported using durations as short as 2 min on neonates (Lee et al., 2020; White et al., 2012), or 100 s in infants (Bulgarelli et al., 2020; Bulgarelli et al., 2019). Wang et al. (2017) reported that 1-min recording segments are enough to obtain FC maps with as high an accuracy as 10 min segments Wang et al., 2017. Our opinion remains, however, that longer data segments are critical, and the conservative nature of our data selection reflects this position.

Another limitation of the current study is that the durations of AS and QS segments extracted for our FC analyses were significantly different. This was almost certainly due to the fact that AS, by definition, will involve more frequent subject motion (see **Supplementary Material** videos) (Scher, 2008), which complicates the extraction of motion-artifact free segments of sufficient duration. While various motion artifact correction approaches are available, their impact on RSFC data in infants are not well known, and therefore we decided to take the most conservative approach of only selecting motion artifact-free segments. Our parameters for motion detection using *hmrMortionArtifact* were also more strict than previous publications. Even with these conservative decisions, we retained 62.2% (28/45) of subjects, which is consistent with the average reported 60% retention rate in most infant fNIRS studies (Lloyd-Fox et al., 2010).

The acquired HD-DOT signal contains representing brain activity as well as processes related to systemic physiological changes (Kirilina et al., 2012). It is important to consider that the effects of RSFC and sleep on the brain cannot be easily disentangled from physiological noise in the signal, and that shifting between sleep and wake itself results in large and widespread physiological changes that can affect RSFC, even after global signal regression (Soon et al., 2021).

Studies of premature newborn infants in intensive care using an adapted version of this system are currently ongoing. Complications related to prematurity, such as white matter injury (Smyser et al., 2013) hemorrhagic parenchymal infarction (Arichi et al., 2014), and exposure to stress and painful procedures (Smith et al., 2011) may affect FC development. Although sleep is the predominant behavioral state in the neonate, the busy environment of the NICU can disrupt sleep organization in both preterm and sick term neonates (Scher et al., 1992; Scher et al., 2002). Future directions also include greater investigation on the effects of motion artifact correction and short separation regression on infant RSFC data. We employed short separation regression by removing the average of all short separation channels, yet validation of this approach in newborn infants, who have smaller heads and shorter scalp-to-brain distances than adults, is clearly needed.

In conclusion, we have demonstrated the feasibility of using a wearable HD-DOT system for cot-side functional neuroimaging of the newborn brain in clinical settings. The system is well-tolerated, adaptable, and easy to apply for long recording durations. We used this system to capture basic features of FC in newborn infants during sleep, and demonstrated differences in FC across newborn sleep states, AS and QS. This work also represents the first study to apply a cortical parcellation scheme for data dimensionality reduction in infant fNIRS data analysis. Given the developments demonstrated here, we believe there is great potential for wearable HD-DOT to become integrated into the clinical setting for studies of brain function in neonatal populations.

Data Availability

The data that has been used is confidential.

Credit authorship contribution statement

Julie Uchitel: Conceptualization, Methodology, Visualization, Formal analysis, Writing – original draft, Writing – review & editing. **Borja Blanco:** Conceptualization, Methodology, Formal analysis, Visualization, Writing – review & editing. **Liam Collins-Jones:** Methodology, Formal analysis, Writing – review & editing. **Jem Hebden:** Conceptualization, Writing – review & editing. **Robert J Cooper:** Investigation, Supervision, Conceptualization, Methodology, Writing – review & editing. **Topun Austin:** Investigation, Supervision, Conceptualization, Methodology, Writing – review & editing.

Acknowledgments

This research was funded by a grant from Action Medical Research (GN2859). The NIHR Cambridge Biomedical Research Centre (BRC) is a partnership between Cambridge University Hospitals NHS Foundation Trust and the University of Cambridge, funded by the National Institute for Health Research (NIHR), TA is supported by the NIHR Cambridge BRC. TA is also supported by the NIHR Brain Injury MedTech Co-operative. JU is supported by a Marshall Scholarship and a Cambridge Trust Scholarship. The views expressed are those of the author(s) and not necessarily those of the NIHR or the Department of Health and Social Care. LCJ is supported by a EPSRC Doctoral Research Fellowship.

Supplementary materials

Supplementary material associated with this article can be found, in the online version, at doi:10.1016/j.neuroimage.2022.119784.

References

Alexander, B., Murray, A.L., Loh, W.Y., et al., 2017. A new neonatal cortical and subcortical brain atlas: the Melbourne children's regional infant brain (M-CRIB) atlas. NeuroImage 147, 841–851. doi:10.1016/j.neuroimage.2016.09.068.

Alexander, B., Loh, W.Y., Matthews, L.G., et al., 2019. Desikan-Killiany-Tourville atlas compatible version of M-CRIB neonatal parcellated whole brain atlas: the M-CRIB 2.0. Front Neurosci 13, 34. doi:10.3389/fnins.2019.00034.

Amico, E., Marinazzo, D., Di Perri, C., et al., 2017. Mapping the functional connectome traits of levels of consciousness. NeuroImage 148, 201–211. doi:10.1016/j.neuroimage.2017.01.020.

Arichi, T., Counsell, S.J., Allievi, A.G., et al., 2014. The effects of hemorrhagic parenchymal infarction on the establishment of sensori-motor structural and functional connectivity in early infancy. Neuroradiology 56 (11), 985–994. doi:10.1007/s00234-014-1412-5.

Arridge, S.R., Schotland, J.C., 2009. Optical tomography: forward and inverse problems. Inverse Probl 25 (12), 123010. doi:10.1088/0266-5611/25/12/123010.

Arridge, S.R., 1999. Optical tomography in medical imaging. Inverse Probl 15 (2), R41–R93. doi:10.1088/0266-5611/15/2/022.

Arthurs, O.J., Edwards, A., Austin, T., Graves, M.J., Lomas, D.J., 2012. The challenges of neonatal magnetic resonance imaging. Pediatr Radiol 42 (10), 1183–1194. doi:10.1007/s00247-012-2430-2.

Avants, B., Epstein, C., Grossman, M., Gee, J., 2008. Symmetric diffeomorphic image registration with cross-correlation: Evaluating automated labeling of elderly and neurodegenerative brain. Med Image Anal 12 (1), 26–41. doi:10.1016/j.media.2007.06.004.

Bevilacqua, F., Piguet, D., Marquet, P., Gross, J.D., Tromberg, B.J., Depeursinge, C., 1999. In vivo local determination of tissue optical properties: applications to human brain. Appl Opt 38 (22), 4939–4950. doi:10.1364/ao.38.004939.

Blanco, B., Molnar, M., Carreiras, M., et al., 2021. Group-level cortical functional connectivity patterns using fNIRS: assessing the effect of bilingualism in young infants. Neurophotonics 8 (02). doi:10.1117/1.NPh.8.2.025011.

Blesa, M., Galdi, P., Cox, S.R., et al., 2021. Hierarchical Complexity of the macro-scale neonatal brain. Cereb Cortex 31 (4), 2071–2084. doi:10.1093/cercor/bhaa345.

Bulgarelli, C., Blasi, A., de Klerk, C.C.J.M., Richards, J.E., Hamilton, A., Southgate, V., 2019. Fronto-temporoparietal connectivity and self-awareness in 18-month-olds: a resting state fNIRS study. Dev Cogn Neurosci 38, 100676. doi:10.1016/j.dcn.2019.100676.

Bulgarelli, C., Klerk, C.C.J.M., Richards, J.E., Southgate, V., Hamilton, A., Blasi, A., 2020. The developmental trajectory of fronto-temporoparietal connectivity as a proxy of the default mode network: a longitudinal fNIRS investigation. Hum Brain Mapp 41 (10), 2717–2740. doi:10.1002/hbm.24974.

Burle, B., Spieser, L., Roger, C., Casini, L., Hasbroucq, T., Vidal, F., 2015. Spatial and temporal resolutions of EEG: Is it really black and white? A scalp current density view. Int J Psychophysiol 97 (3), 210–220. doi:10.1016/j.ijpsycho.2015.05.004.

Caballero-Gaudes, C., Reynolds, R.C., 2017. Methods for cleaning the BOLD fMRI signal. NeuroImage 154, 128–149. doi:10.1016/j.neuroimage.2016.12.018.

Chalia, M., Dempsey, L.A., Cooper, R.J., et al., 2019. Diffuse optical tomography for the detection of perinatal stroke at the cot side: a pilot study. Pediatr Res 85 (7), 1001–1007. doi:10.1038/s41390-018-0263-x.

Cho, J.W., Korchmaros, A., Vogelstein, J.T., Milham, M.P., Xu, T., 2021. Impact of concatenating fMRI data on reliability for functional connectomics. NeuroImage 226, 117549. doi:10.1016/j.neuroimage.2020.117549.

Collins-Jones, L.H., Arichi, T., Poppe, T., et al., 2021. Construction and validation of a database of head models for functional imaging of the neonatal brain. Hum Brain Mapp 42 (3), 567–586. doi:10.1002/hbm.25242.

Cope, M., 1991. The development of a near infrared spectroscopy system and its application for non invasive monitoring of cerebral blood and tissue oxygenation in the newborn infants. Doctoral. University of London Accessed January 6, 2021.

Costeloe, K.L., Hennessy, E.M., Haider, S., Stacey, F., Marlow, N., Draper, E.S., 2012. Short term outcomes after extreme preterm birth in England: comparison of two birth cohorts in 1995 and 2006 (the EPICure studies). BMJ 345 (dec04 3), e7976. doi:10.1136/bmj.e7976, -e7976.

Damoiseaux, J.S., Rombouts, S.A., Barkhof F, R.B., et al., 2006. Consistent resting-state networks across healthy subjects. Proc Natl Acad Sci USA 103 (37), 13848–13853. doi:10.1073/pnas.0601417103.

Dereymaeker, A., Pillay, K., Vervisch, J., et al., 2017. Review of sleep-EEG in preterm and term neonates. Early Hum Dev 113, 87–103. doi:10.1016/j.earlhumdev.2017.07.003.

Di Lorenzo, R., Pirazzoli, L., Blasi, A., et al., 2019. Recommendations for motion correction of infant fNIRS data applicable to multiple data sets and acquisition systems. NeuroImage 200, 511–527. doi:10.1016/j.neuroimage.2019.06.056.

Doria, V., Beckmann, C.F., Arichi, T., et al., 2010. Emergence of resting state networks in the preterm human brain. Proc Natl Acad Sci USA 107 (46), 20015–20020. doi:10.1073/pnas.1007921107.

Eggebrecht, A.T., Ferradal, S.L., Robichaux-Viehoever, A., et al., 2014. Mapping distributed brain function and networks with diffuse optical tomography. Nat Photonics 8 (6), 448–454. doi:10.1038/nphoton.2014.107.

Fenchel, D., Dimitrova, R., Seidlitz, J., et al., 2020. Development of microstructural and morphological cortical profiles in the neonatal brain. Cereb Cortex 30 (11), 5767–5779. doi:10.1093/cercor/bhaa150.

Ferradal, S.L., Liao, S.M., Eggebrecht, A.T., et al., 2016. Functional imaging of the developing brain at the bedside using diffuse optical tomography. Cereb Cortex 26 (4), 1558–1568. doi:10.1093/cercor/bhu320, N Y N 1991.

SL. Ferradal Diffuse Optical Tomography Methods for imaging the developing brain. Published online 2014. doi:10.7936/K7NC5Z63

Fransson, P., Skiöld, B., Horsch, S., et al., 2007. Resting-state networks in the infant brain. Proc Natl Acad Sci USA 104 (39), 15531–15536. doi:10.1073/pnas.0704380104.

Frijia, E.M., Billing, A., Lloyd-Fox, S., et al., 2021. Functional imaging of the developing brain with wearable high-density diffuse optical tomography: a new benchmark for infant neuroimaging outside the scanner environment. NeuroImage 225, 117490. doi:10.1016/j.neuroimage.2020.117490.

Fuchino, Y., Naoi, N., Shibata, M., et al., 2013. Effects of preterm birth on intrinsic fluctuations in neonatal cerebral activity examined using optical imaging. PloS One 8 (6), e67432. doi:10.1371/journal.pone.0067432.

Funane, T., Atsumori, H., Katura, T., et al., 2014. Quantitative evaluation of deep and shallow tissue layers' contribution to fNIRS signal using multi-distance optodes and independent component analysis. NeuroImage 85, 150–165. doi:10.1016/j.neuroimage.2013.02.026.

Gagnon, L., Cooper, R.J., Yücel, M.A., Perdue, K.L., Greve, D.N., Boas, DA., 2012. Short separation channel location impacts the performance of short channel regression in NIRS. Neuroimage 59 (3), 2518–2528. doi:10.1016/j.neuroimage.2011.08.095.

Gordon, E.M., Laumann, T.O., Adeyemo, B., Huckins, J.F., Kelley, W.M., Petersen, SE., 2016. Generation and evaluation of a cortical area parcellation from resting-state correlations. Cereb Cortex 26 (1), 288–303. doi:10.1093/cercor/bhu239.

Gregg, 2010. Brain specificity of diffuse optical imaging: improvements from superficial signal regression and tomography. Front Neuroenergetics doi:10.3389/fnene.2010.00014, Published online.

Hakamada, S., Watanabe, K., Hara, K., Miyazaki, S., 1981. Development of the motor behavior during sleep in newborn infants. Brain Dev 3 (4), 345–350. doi:10.1016/S0387-7604(81)80062-9.

Homae, F., Watanabe, H., Otobe, T., et al., 2010. Development of global cortical networks in early infancy. J Neurosci Off J Soc Neurosci 30 (14), 4877–4882. doi:10.1523/JNEUROSCI.5618-09.2010.

Homae, F., Watanabe, H., Nakano, T., Taga, G., 2011. Large-scale brain networks underlying language acquisition in early infancy. Front Psychol 2, 93. doi:10.3389/fpsyg.2011.00093.

Huppert, T.J., Diamond, S.G., Franceschini, M.A., Boas, DA., 2009. HomER: a review of time-series analysis methods for near-infrared spectroscopy of the brain. Appl Opt 48 (10), D280–D298. doi:10.1364/ao.48.00d280.

Hyvärinen, A., Oja, E., 2000. Independent component analysis: algorithms and applications. Neural Netw 13 (4-5), 411–430. doi:10.1016/S0893-6080(00)00026-5.

Imai, M., Watanabe, H., Yasui, K., et al., 2014. Functional connectivity of the cortex of term and preterm infants and infants with Down's syndrome. NeuroImage 85, 272–278. doi:10.1016/j.neuroimage.2013.04.080.

Kirilina, E., Jelzow, A., Heine, A., et al., 2012. The physiological origin of task-evoked systemic artefacts in functional near infrared spectroscopy. NeuroImage 61 (1), 70–81. doi:10.1016/j.neuroimage.2012.02.074.

Lee, C.W., Blanco, B., Dempsey, L., et al., 2020. Sleep state modulates resting-state functional connectivity in neonates. Front Neurosci 14, 347. doi:10.3389/fnins.2020.00347.

Lewis, J.D., Bezgin, G., Fonov, V.S., Collins, D.L., Evans, A.C., 2022. A sub+cortical fMRI-based surface parcellation. Hum Brain Mapp 43 (2), 616–632. doi:10.1002/hbm.25675.

Liao, S.M., Ferradal, S.L., White, B.R., Gregg, N., Inder, T.E., Culver, J.P., 2012. High-density diffuse optical tomography of term infant visual cortex in the nursery. J Biomed Opt 17 (8), 081414. doi:10.1117/1.JBO.17.8.081414.

Lloyd-Fox, S., Blasi, A., Elwell, C.E., 2010. Illuminating the developing brain: the past, present and future of functional near infrared spectroscopy. Neurosci Biobehav Rev 34 (3), 269–284. doi:10.1016/j.neubiorev.2009.07.008.

Makropoulos, A., Gousias, I.S., Ledig, C., et al., 2014. Automatic whole Brain MRI segmentation of the developing neonatal brain. IEEE Trans Med Imaging 33 (9), 1818–1831. doi:10.1109/TMI.2014.2322280.

Makropoulos, A., Robinson, E.C., Schuh, A., et al., 2018. The developing human connectome project: a minimal processing pipeline for neonatal cortical surface reconstruction. NeuroImage 173, 88–112. doi:10.1016/j.neuroimage.2018.01.054.

Mesquita, R.C., Franceschini, M.A., Boas, D.A., 2010. Resting state functional connectivity of the whole head with near-infrared spectroscopy. Biomed Opt Express 1 (1), 324–336. doi:10.1364/BOE.1.000324.

Mirmiran, M., Maas, Y.G.H., Ariagno, R.L., 2003. Development of fetal and neonatal sleep and circadian rhythms. Sleep Med Rev 7 (4), 321–334. doi:10.1053/smrv.2002.0243.

Morrison, J.L., Carmichael, L., Homan, J., White, S., Richardson, BS., 2005. Cerebral blood flow during spontaneous and cholinergically induced behavioral states in the sheep fetus. Pediatr Res 57 (5 Part 1), 667–673. doi:10.1203/01.PDR.0000156210.27381.12.

Naoi, N., Fuchino, Y., Shibata, M., et al., 2013. Decreased right temporal activation and increased interhemispheric connectivity in response to speech in preterm infants at term-equivalent age. Front Psychol 4, 94. doi:10.3389/fpsyg.2013.00094.

Pinti, P., Tachtsidis, I., Hamilton, A., et al., 2020. The present and future use of functional near-infrared spectroscopy (fNIRS) for cognitive neuroscience. Ann N Y Acad Sci 1464 (1), 5–29. doi:10.1111/nyas.13948.

Quaresima, V., Bisconti, S., Ferrari, M., 2012. A brief review on the use of functional near-infrared spectroscopy (fNIRS) for language imaging studies in human newborns and adults. Brain Lang 121 (2), 79–89. doi:10.1016/j.bandl.2011.03.009.

Saager, R., Berger, A., 2008. Measurement of layer-like hemodynamic trends in scalp and cortex: implications for physiological baseline suppression in functional near-infrared spectroscopy. J Biomed Opt 13 (3), 034017. doi:10.1117/1.2940587.

Santosa, H., Aarabi, A., Perlman, S.B., Huppert, T.J., 2017. Characterization and correction of the false-discovery rates in resting state connectivity using functional near-infrared spectroscopy. J Biomed Opt 22 (5), 55002. doi:10.1117/1.JBO.22.5.055002.

Sato, T., Nambu, I., Takeda, K., et al., 2016. Reduction of global interference of scalp-hemodynamics in functional near-infrared spectroscopy using short distance probes. NeuroImage 141, 120–132. doi:10.1016/j.neuroimage.2016.06.054.

Schaefer, A., Kong, R., Gordon, E.M., et al., 2018. Local-Global parcellation of the human cerebral cortex from intrinsic functional connectivity MRI. Cereb Cortex 28 (9), 3095–3114. doi:10.1093/cercor/bhx179.

Scher, M.S., Steppe, D.A., Dahl, R.E., Asthana, S., Guthrie, R.D., 1992. Comparison of EEG sleep measures in healthy full-term and preterm infants at matched conceptional ages. Sleep 15 (5), 442–448. doi:10.1093/sleep/15.5.442.

Scher, M.S., Steppe, D.A., Beggarly, M.E., Salerno, D.G., Banks, D.L., 2002. Neonatal EEG-sleep disruption mimicking hypoxic-ischemic encephalopathy after intrapartum asphyxia. Sleep Med 3 (5), 411–415. doi:10.1016/S1389-9457(02)00071-0.

Scher, M.S., 2008. Ontogeny of EEG-sleep from neonatal through infancy periods. Sleep Med 9 (6), 615–636. doi:10.1016/j.sleep.2007.08.014.

Scholkmann, F., Kleiser, S., Metz, A.J., et al., 2014. A review on continuous wave functional near-infrared spectroscopy and imaging instrumentation and methodology. NeuroImage 85, 6–27. doi:10.1016/j.neuroimage.2013.05.004.

Schweiger, M., Arridge, S., 2003. Image reconstruction in optical tomography using local basis functions. J Electron Imaging 12, 583–593. doi:10.1117/1.1586919.

Schweiger, M., Arridge, S., 2014. The Toast++ software suite for forward and inverse modeling in optical tomography. J Biomed Opt 19 (4), 040801. doi:10.1117/1.JBO.19.4.040801.

Shellhaas, R.A., Burns, J.W., Hassan, F., Carlson, M.D., Barks, J.D.E., Chervin, R.D., 2017. Neonatal sleep-wake analyses predict 18-month neurodevelopmental outcomes. Sleep 40 (11). doi:10.1093/sleep/zsx144.

Shi, F., Salzwedel, A.P., Lin, W., Gilmore, J.H., Gao, W., 2018. Functional brain parcellations of the infant brain and the associated developmental trends. Cereb Cortex 28 (4), 1358–1368. doi:10.1093/cercor/bhx062.

Silvani, A., Asti, V., Berteotti, C., et al., 2006. Sleep-dependent changes in cerebral oxygen consumption in newborn lambs. J Sleep Res 15 (2), 206–211. doi:10.1111/j.1365-2869.2006.00521.x.

Singh, H., Cooper, R.J., Wai Lee, C., et al., 2014. Mapping cortical haemodynamics during neonatal seizures using diffuse optical tomography: a case study. NeuroImage Clin 5, 256–265. doi:10.1016/j.nicl.2014.06.012.

Slupe, A.M., Kirsch, J.R., 2018. Effects of anesthesia on cerebral blood flow, metabolism, and neuroprotection. J Cereb Blood Flow Metab 38 (12), 2192–2208. doi:10.1177/0271678X18789273.

Smith, G.C., Gutovich, J., Smyser, C., et al., 2011. Neonatal intensive care unit stress is associated with brain development in preterm infants. Ann Neurol 70 (4), 541–549. doi:10.1002/ana.22545.

Smyser, C.D., Inder, T.E., Shimony, J.S., et al., 2010. Longitudinal analysis of neural network development in preterm infants. Cereb Cortex 20 (12), 2852–2862. doi:10.1093/cercor/bhq035.

Smyser, C.D., Snyder, A.Z., Shimony, J.S., Blazey, T.M., Inder, T.E., Neil, JJ., 2013. Effects of white matter injury on resting state fMRI measures in prematurely born infants. fan Y, ed. PLoS ONE 8 (7), e68098. doi:10.1371/journal.pone.0068098.

Soon, C.S., Vinogradova, K., Ong, J.L., et al., 2021. Respiratory, cardiac, EEG, BOLD signals and functional connectivity over multiple microsleep episodes. NeuroImage 237, 118129. doi:10.1016/j.neuroimage.2021.118129.

Stangenes, K.M., Fevang, S.K., Grundt, J., et al., 2017. Children born extremely preterm had different sleeping habits at 11 years of age and more childhood sleep problems than term-born children. Acta Paediatr 106 (12), 1966–1972. doi:10.1111/apa.13991.

Strangman, G., Franceschini, M.A., Boas, D.A., 2003. Factors affecting the accuracy of near-infrared spectroscopy concentration calculations for focal changes in oxygenation parameters. NeuroImage 18 (4), 865–879. doi:10.1016/S1053-8119(03)00021-1.

Tokariev, A., Videman, M., Palva, J.M., Vanhatalo, S., 2016. Functional brain connectivity develops rapidly around term age and changes between vigilance states in the human newborn. Cereb Cortex 26 (12), 4540–4550. doi:10.1093/cercor/bhv219, N Y N 1991.

Tokariev, A., Roberts, J.A., Zalesky, A., et al., 2019. Large-scale brain modes reorganize between infant sleep states and carry prognostic information for preterms. Nat Commun 10 (1), 2619. doi:10.1038/s41467-019-10467-8.

Vidal-Rosas, E.E., Zhao, H., Nixon-Hill, R.W., et al., 2021. Evaluating a new generation of wearable high-density diffuse optical tomography technology via retinotopic mapping of the adult visual cortex. Neurophotonics 8 (2), 025002. doi:10.1117/1.NPh.8.2.025002.

Wang, H., Suh, J.W., Das, S.R., Pluta, J.B., Craige, C., Yushkevich, PA., 2013. Multi-atlas segmentation with joint label fusion. IEEE Trans Pattern Anal Mach Intell 35 (3), 611–623. doi:10.1109/TPAMI.2012.143.

Wang, J., Dong, Q., Niu, H., 2017. The minimum resting-state fNIRS imaging duration for accurate and stable mapping of brain connectivity network in children. Sci Rep 7 (1), 6461. doi:10.1038/s41598-017-06340-7.

White, B.R., Culver, J.P., 2010. Quantitative evaluation of high-density diffuse optical tomography: in vivo resolution and mapping performance. J Biomed Opt 15 (2), 026006. doi:10.1117/1.3368999.

White, B.R., Snyder, A.Z., Cohen, A.L., et al., 2009. Resting-state functional connectivity in the human brain revealed with diffuse optical tomography. NeuroImage 47 (1), 148–156. doi:10.1016/j.neuroimage.2009.03.058.

White, B.R., Liao, S.M., Ferradal, S.L., Inder, T.E., Culver, J.P., 2012. Bedside optical imaging of occipital resting-state functional connectivity in neonates. NeuroImage 59 (3), 2529–2538. doi:10.1016/j.neuroimage.2011.08.094.

Wielek, T., Del Giudice, R., Lang, A., Wislowska, M., Ott, P., Schabus, M., 2019. On the development of sleep states in the first weeks of life. PloS One 14 (10), e0224521. doi:10.1371/journal.pone.0224521.